A New Methodology Based on an Iterative Multiscaling for Microwave Imaging

Salvatore Caorsi, *Member, IEEE*, Massimo Donelli, Davide Franceschini, and Andrea Massa, *Member, IEEE*

***Abstract*—In this paper, the problem of the localization, shaping, and dielectric permittivity reconstruction of dielectric targets is addressed. The scatterers under test are inhomogeneous cylinders of arbitrary cross sections probed by a set of incident electromagnetic fields of TM type. The scattered field data are processed in order to locate and roughly recover the objects' shapes. The scatterers under test are then reconstructed with an increasing accuracy by means of an iterative multiscaling procedure until stationary reconstructions are achieved. The proposed method is presented jointly with a modified conjugate-gradient inversion procedure in order to minimize the rising cost function. However, this methodology is independent from the minimization algorithm, and other and more efficient algorithms can be used. In order to assess the effectiveness of the iterative multiscaling method, the results of several test cases (with and without noise) are presented and discussed in more detail.**

***Index Terms*—Inverse scattering, iterative multiscaling method, microwave imaging.**

I. Introduction

THE problem of the localization and dielectric reconstruction of unknown targets from the measurement of the scattered field is a topic of great interest in the framework of microwave imaging techniques (see [13]) based on inverse-scattering methodologies [1]–[3]. Moreover, many problems occurring in various areas of applied science, such as biomedical engineering [5], medicine [6], [7], nondestructive testing for the industrial production [8], and buried-object detection and reconstruction [9]–[11] can be mathematically formulated as inverse-scattering problems (see [12] for a complete overview). However, severe limitations in obtaining accurate reconstructions are due to some intrinsic drawbacks of the inverse-scattering problem [14], [15] jointly with the feasibility of efficient illumination and measurements systems. By a mathematical point-of-view, three main topics must be preliminary addressed in order to define an efficient reconstruction procedure: the uniqueness of the solution, the ill-posedness, and the intrinsic nonlinearity of the problems. As far as the uniqueness is concerned, the dielectric profile of the object under test results is uniquely defined only if pressing requirements (very difficult to be achieved in real situations) are verified [16], [17]. Generally speaking, the nonuniqueness and the ill-posedness drawbacks of the inverse problem are due to the limited amount of information that can be collected. In fact, the number of independent data achievable from the measurements of the scattered field is essentially limited [24]. It leads to the conclusion that the space of the unknown is of finite dimension and, consequently, only a finite number of parameters of the unknown contrast can be accurately retrieved. In order to recover a solution of the inverse-scattering problem, a generalized solution is then defined by searching for approximate solutions satisfying additional constraints coming from the physics of the problem. This additional information is necessary in order to compensate for the loss of information due to the imaging process [25]. To this end, a suitable cost functional is defined, whose global minimum is assumed as the reconstructed profile.

On the other hand, due to the multiple scattering phenomena, the inverse-scattering problem results in nonlinearity [15], as well as a rising cost function. The nonlinearity can be avoided for certain limited real cases for which a linear relationship between the scattered field and object under test can be found [18]. However, when multiple scattering effects are not negligible, as is the case for large or highly contrasted objects, the use of nonlinear methodologies is mandatory. Many very effective optimization strategies have been proposed. These techniques can be grouped into deterministic (e.g., the modified gradient approach [19] or the distorted-Born iterative method [20]) or stochastic methods (e.g., the simulated-annealing procedure [21] or the genetic-algorithm-based approaches [22]).

This paper presents a method located in the framework of optimization techniques and is aimed at better exploiting all the available information. Analogously to standard optimization techniques, the proposed methodology uses the additional information (expressed in the form of constraints on the solution) at the start of the iterative procedure to construct approximate solutions. However, successively the procedure iterates a sort of zoom inside the investigation domain, introducing a sort of "acquired" information about the scatterer under test (information achieved at the previous reconstruction steps). This helps to locate the scatterer inside the investigation domain and, at the same time, to reallocate all the available *a priori* information in order to achieve a finer reconstruction.

In the following sections, the proposed technique will be widely illustrated. After the mathematical statement of the problem and an analytical description of the iterative multiscaling procedure (Section II), some numerical experiments will be shown in Section III. Dielectric scatterers in various shapes, dimensions, and permittivities will be considered in order to accurately evaluate current potentialities of the proposed method. Finally (Section IV), some conclusions will be drawn and possible future developments pointed out.

Manuscript received January 30, 2002; revised November 4, 2002.

S. Caorsi is with the Department of Electronics, University of Pavia, I-422583 Pavia, Italy.

M. Donelli, D. Franceschini, and A. Massa are with the Department of Information and Communication Technology, University of Trento, I-38050 Trento, Italy.

Digital Object Identifier 10.1109/TMTT.2003.809677

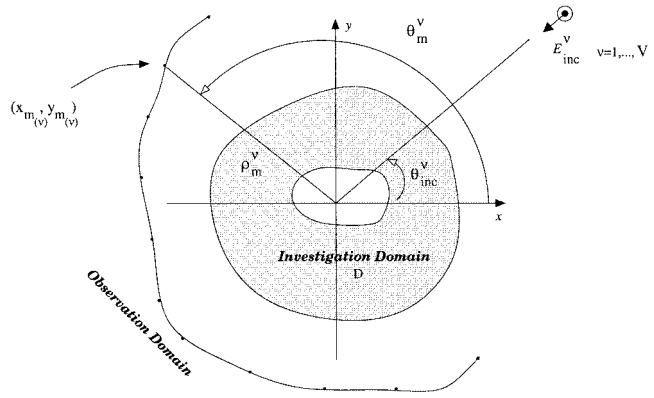

Fig. 1. Imaging configuration.

II. Mathematical Formulation

Let us consider a cylindrical object belonging to an investigation domain D (Fig. 1). The target is illumined by a finite set of incident electromagnetic fields of TM type ($\mathbf{E}^v_{\mathbf{inc}}(\mathbf{r}) = E^v_{\mathbf{inc}}(x,y)\hat{\mathbf{z}};\ v = 1,\ldots,V$). The scattered electric field is collected at $M^{(v)}$ different measurement points, located in an observation domain D_{obs} external to the investigation domain ($\mathbf{E}^v_{\mathrm{scatt}}(\mathbf{r}) = E^v_{\mathrm{scatt}}(x_{m_{(v)}}, y_{m_{(v)}})\hat{\mathbf{z}};\ m_{(v)} = 1,\ldots,M^{(v)}$).

The material properties of the dielectric object are modeled by means of an object function $\tau(x,y)$ defined as follows:

$$\tau(x,y) = \varepsilon_r(x,y) - 1 - j\frac{\sigma(x,y)}{2\pi f \varepsilon_0} \tag{1}$$

with $\varepsilon_r(x,y)$ and $\sigma(x,y)$ being the dielectric permittivity and electric conductivity, respectively. A lossless nonmagnetic background medium, characterized by a dielectric permittivity ε_0, is assumed. The interactions between scatterer and probing electromagnetic fields are described by means of the inverse-scattering equations [26]. In order to numerically solve the addressed inverse-scattering problem, the inverse-scattering equations are discretized according to the well-known Richmond's procedure [27]. The investigation domain D is discretized into N square subdomains. The electric field and object function are constant quantities in each subdomain and are equal to $E^v_{\mathrm{tot}}(x_n, y_n)$ and $\tau(x_n, y_n)$, respectively. Generally, in order to obtain a solution of the rising multiobjective problem, a suitable cost function is defined as the measure of the errors in the *data equation* and *state equation* [26]. Successively the cost function is minimized according to an optimization strategy [21], [29], [30], [31]. The proposed methodology is independent from the definition of the cost function and also from the minimization algorithm. The method is aimed at better resolving the object function distribution by considering a multiresolution iterative process. At the first step of the inversion procedure ($s = 1$), a "coarse" profile of the object function distribution is looked for and the same resolution level, $R = 1$ (R being the index of the resolution level), is considered in any part of the investigation domain. On the basis of the first reconstruction, a "zoom" (by using the *acquired a priori information* about the scenario under test) is then performed in the region where the unknown scatterer has been detected. Iteratively, the procedure is repeated until a "stationary" reconstruction is achieved. In more detail, at each step of the iterative process, by means of the *acquired a priori information* (achieved at the previous steps), the scatterer under test is localized and a zoomed square investigation domain $D_{(s-1)}$ is centered at

$$x_{c_{(s-1)}} = \frac{\sum_{r=1}^{R}\sum_{n_{(r)}=1}^{N_{(r)}}\left\{x_{n_{(r)}}\tau\left(x_{n_{(r)}}, y_{n_{(r)}}\right)\right\}}{\sum_{n_{(r)}=1}^{N_{(r)}}\left\{\tau\left(x_{n_{(r)}}, y_{n_{(r)}}\right)\right\}}, \qquad R = s-1$$

$$y_{c_{(s-1)}} = \frac{\sum_{r=1}^{R}\sum_{n_{(r)}=1}^{N_{(r)}}\left\{y_{n_{(r)}}\tau\left(x_{n_{(r)}}, y_{n_{(r)}}\right)\right\}}{\sum_{n_{(r)}=1}^{N_{(r)}}\left\{\tau\left(x_{n_{(r)}}, y_{n_{(r)}}\right)\right\}}. \tag{2}$$

$L_{(s-1)}$ inside

$$L_{(s-1)} = 2\frac{\sum_{r=1}^{R}\sum_{n_{(r)}=1}^{N_{(r)}}\left\{\dfrac{\rho_{n_{(r)}c_{(s-1)}}\tau\left(x_{n_{(r)}}, y_{n_{(r)}}\right)}{\max_{n_{(r)}=1,\ldots,N_{(r)}}\left\{\tau\left(x_{n_{(r)}}, y_{n_{(r)}}\right)\right\}}\right\}}{\sum_{r=1}^{R}\sum_{n_{(r)}=1}^{N_{(r)}}\left\{\dfrac{\tau\left(x_{n_{(r)}}, y_{n_{(r)}}\right)}{\max_{n_{(r)}=1,\ldots,N_{(r)}}\left\{\tau\left(x_{n_{(r)}}, y_{n_{(r)}}\right)\right\}}\right\}} \tag{3}$$

is defined as being $(x_{n_{(r)}}, y_{n_{(r)}})$ the center of the square subdomain ($l_{(r)}$-sided). According to a multiresolution strategy, a higher resolution level ($R = s$) is adopted only for the reduced investigation domain. $D_{(s-1)}$ is discretized in the N_R square subdomain l_r-sided ($l_r < l_{(r-1)}$). The number of discretization domains is chosen equal to the essential dimension of the scattered data. The upgraded permittivity profile is then retrieved by minimizing the multiresolution cost function $\Phi^{(s)}$, defined as shown in (4), at the bottom of the following page, where $G_{2d}\left(A_{q_{(r)}}, \rho_{q_{(r)}n_{(r)}}\right)$ and $G_{2d}\left(A_{n_{(r)}}, \rho_{n_{(r)}m_{(v)}}\right)$ indicate the discretized forms of the Green integrals given in [31, eq. (5)] being $\rho_{n_{(r)}m_{(v)}} = \sqrt{\left(x_{n_{(r)}} - x_{m_{(v)}}\right)^2 + \left(y_{n_{(r)}} - y_{m_{(v)}}\right)^2}$, $\rho_{q_{(r)}n_{(r)}} = \sqrt{\left(x_{q_{(r)}} - x_{n_{(r)}}\right)^2 + \left(y_{q_{(r)}} - y_{n_{(r)}}\right)^2}$, and $A_{n_{(r)}} = \left(l_{(r)}\right)^2$ the area of the nth cell at the Rth resolution level. Moreover, w is a weighting function, which is defined as follows:

$$w\left(x_{n_{(r)}}, y_{n_{(r)}}\right) = \begin{cases} 0, & \text{if } \left(x_{n_{(r)}}, y_{n_{(r)}}\right) \notin D_{(s-1)} \\ 1, & \text{if } \left(x_{n_{(r)}}, y_{n_{(r)}}\right) \in D_{(s-1)}. \end{cases} \tag{5}$$

The multiresolution procedure is iterated until a "stationary condition" for the quantitative imaging of the scatterer under test is achieved ($s = S_{\mathrm{opt}}$). This condition hold when

$$\eta_x^{(s)} = \left\{\frac{\left|x_c^{(s+1)} - x_c^{(s)}\right|}{\left|x_c^{(s+1)}\right|} \times 100\right\} < \eta_x \tag{6}$$

$$\eta_y^{(s)} = \left\{ \frac{\left| y_c^{(s+1)} - y_c^{(s)} \right|}{\left| y_c^{(s+1)} \right|} \times 100 \right\} < \eta_y \tag{7}$$

and

$$\eta_L^{(s)} = \left\{ \frac{\left| L_{(s+1)} - L_{(s)} \right|}{L_{(s+1)}} \times 100 \right\} < \eta_L. \tag{8}$$

Fig. 2 summarizes the iterative multiresolution procedure by means of a pictorial representation.

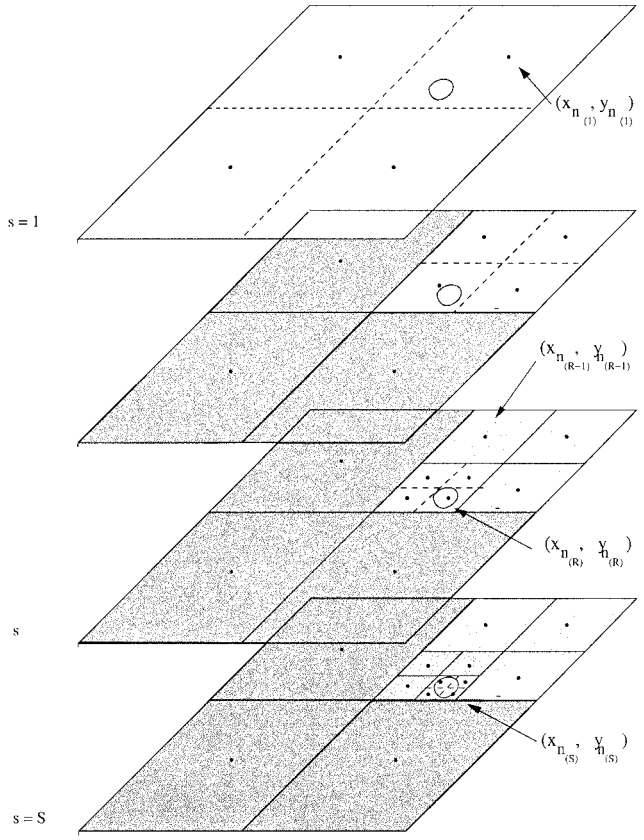

Fig. 2. Iterative multiresolution schema.

III. Numerical Results

In this section, in order to asses the effectiveness of the proposed method, the results of several numerical simulations are reported. The behavior of the proposed method is illustrated by considering three different class of scatterers: irregular homogeneous scatterers, circular homogeneous scatterers, and inhomogeneous scatterers.

A. Definitions

Before presenting the set of illustrative test cases, some quantities, used in the numerical analysis, are defined. In order to evaluate the local and global reconstruction accuracy, let us consider the following error figures:

$$\gamma_{(j)} = \sum_{r=1}^{R} \frac{1}{N_{(r)}^{(j)}} \sum_{n_{(r)}=1}^{N_{(r)}^{(j)}} \left\{ \frac{\tau\left(x_{n_{(r)}}, y_{n_{(r)}}\right) - \tau^{\mathrm{ref}}\left(x_{n_{(r)}}, y_{n_{(r)}}\right)}{\tau^{\mathrm{ref}}\left(x_{n_{(r)}}, y_{n_{(r)}}\right)} \right\} \times 100, \qquad R = S_{\mathrm{opt}} \tag{9}$$

where τ and τ^{ref} are the values of the actual and reconstructed object function, respectively; $N_{(r)}^{(j)}$ can range over the whole investigation domain ($j \Rightarrow \mathrm{tot}$), or over the area where the actual scatterer is located ($j \Rightarrow \mathrm{int}$), or over the background belonging to the investigation domain ($j \Rightarrow \mathrm{ext}$). Moreover, let us define the "*local error*"

$$\chi_{n_{(r)}} = \frac{\left| \tau\left(x_{n_{(r)}}, y_{n_{(r)}}\right) - \tau^{\mathrm{ref}}\left(x_{n_{(r)}}, y_{n_{(r)}}\right) \right|}{\left| \tau^{\mathrm{ref}}\left(x_{n_{(r)}}, y_{n_{(r)}}\right) \right|} \times 100 \tag{10}$$

for each discretization cell of the investigation domain.

$$\begin{aligned}
&\Phi^{(s)}\left\{ \tau\left(x_{n_{(r)}}, y_{n_{(r)}}\right) \quad E_{\mathrm{tot}}^{v}\left(x_{n_{(r)}}, y_{n_{(r)}}\right), \qquad r = 1, \ldots, R = s; \quad n_{(r)} = 1, \ldots, N_{(r)}; \quad v = 1, \ldots, V \right\} \\
&= \left\{ \sum_{v=1}^{V} \sum_{m=1}^{M} \left| E_{\mathrm{scatt}}^{v}\left(x_{m_{(v)}}, y_{m_{(v)}}\right) \sum_{r=1}^{R} \sum_{n_{(r)}=1}^{N_{(r)}} \left\{ w\left(x_{n_{(r)}}, y_{n_{(r)}}\right) \tau\left(x_{n_{(r)}}, y_{n_{(r)}}\right) E_{\mathrm{tot}}^{v}\left(x_{n_{(r)}}, y_{n_{(r)}}\right) G_{2d}\left(A_{n_{(r)}}, \rho_{n_{(r)} m_{(v)}}\right) \right\} \right|^2 \right\} \\
&\quad + \left\{ \sum_{v=1}^{V} \sum_{r=1}^{R} \sum_{n_{(r)}=1}^{N_{(r)}} \left\{ w\left(x_{n_{(r)}}, y_{n_{(r)}}\right) \right. \right. \\
&\qquad \left. \left. \cdot \left| E_{\mathrm{inc}}^{v}\left(x_{n_{(r)}}, y_{n_{(r)}}\right) - \left[E_{\mathrm{tot}}^{v}\left(x_{n_{(r)}}, y_{n_{(r)}}\right) \right. \right. \right. \right. \\
&\qquad \left. \left. \left. \left. + \sum_{q_{(r)}=1}^{N_{(r)}} \left\{ \tau\left(x_{q_{(r)}}, y_{q_{(r)}}\right) E_{\mathrm{tot}}^{v}\left(x_{q_{(r)}}, y_{q_{(r)}}\right) G_{2d}\left(A_{q_{(r)}}, \rho_{q_{(r)} n_{(r)}}\right) \right\} \right] \right| \right\}^2 \right\}
\end{aligned} \tag{4}$$

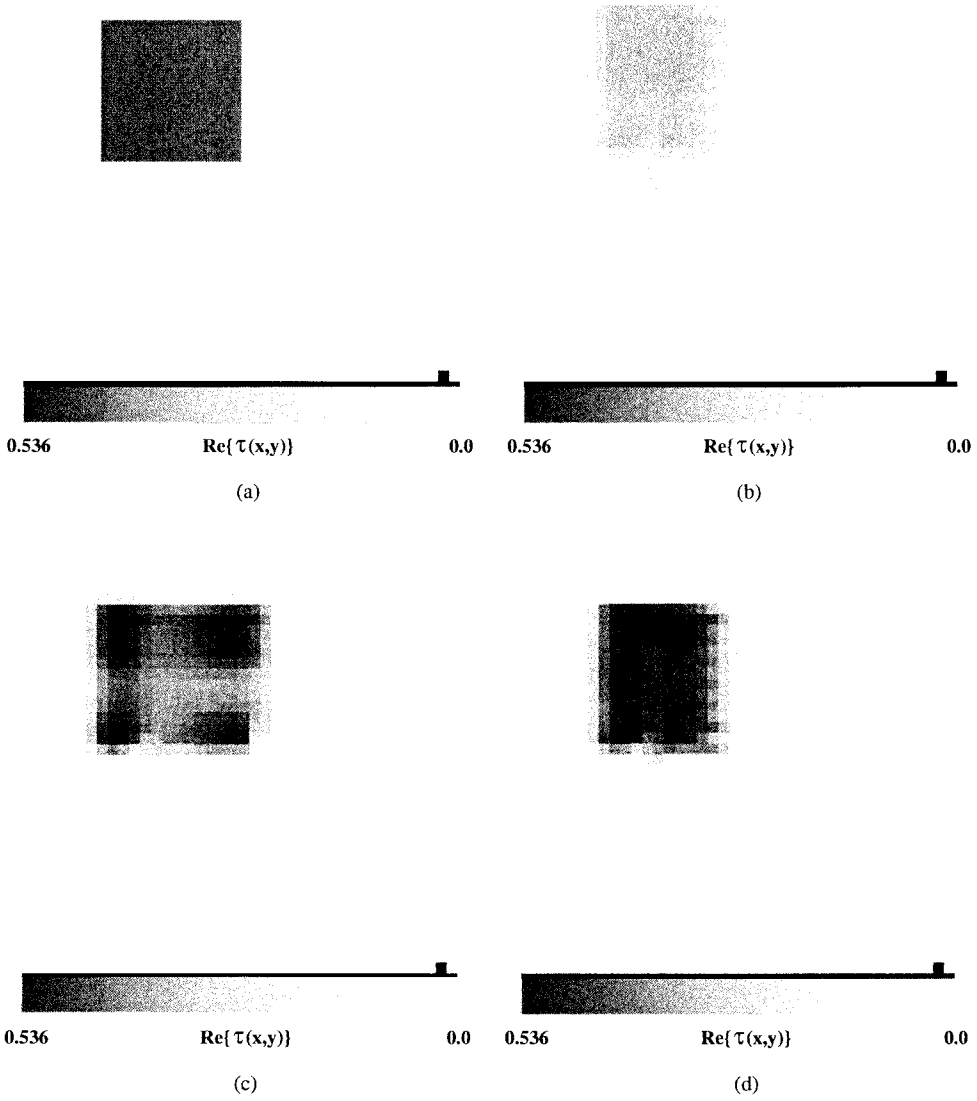

Fig. 3. Reconstruction of an off-centered square homogeneous cylinder. (a) Reference distribution. Reconstruction at intermediate steps: (b) $s = 1$, (c) $s = 2$. (d) Final convergent profile ($s = S_{\rm opt} = 3$).

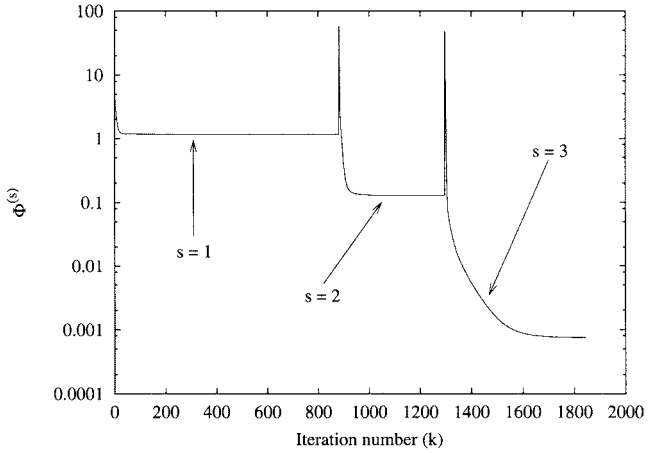

Fig. 4. Reconstruction of an off-centered square homogeneous cylinder. Behavior of the multiresolution cost function.

TABLE I
RECONSTRUCTION OF AN OFF-CENTERED SQUARE HOMOGENEOUS CYLINDER. LOCATION AND SHAPE PARAMETERS

Step No. (s)	*0*	*1*	*2*	*3*	*4*
$\frac{x_{c_{(s)}}}{\lambda_0}$	0.0	−0.220	−0.380	−0.397	−0.397
$\frac{y_{c_{(s)}}}{\lambda_0}$	0.0	0.220	0.380	0.397	0.397
$\frac{L_{(s)}}{2\lambda_0}$	1.2	0.880	0.540	0.430	0.420

TABLE II
RECONSTRUCTION OF AN OFF-CENTERED SQUARE HOMOGENEOUS CYLINDER. ERROR FIGURES

Step No. (s)	*1*	*2*	*3*
γ_{tot}	4.37	0.82	0.12
γ_{int}	11.25	5.80	1.10
γ_{ext}	3.52	0.20	0.01

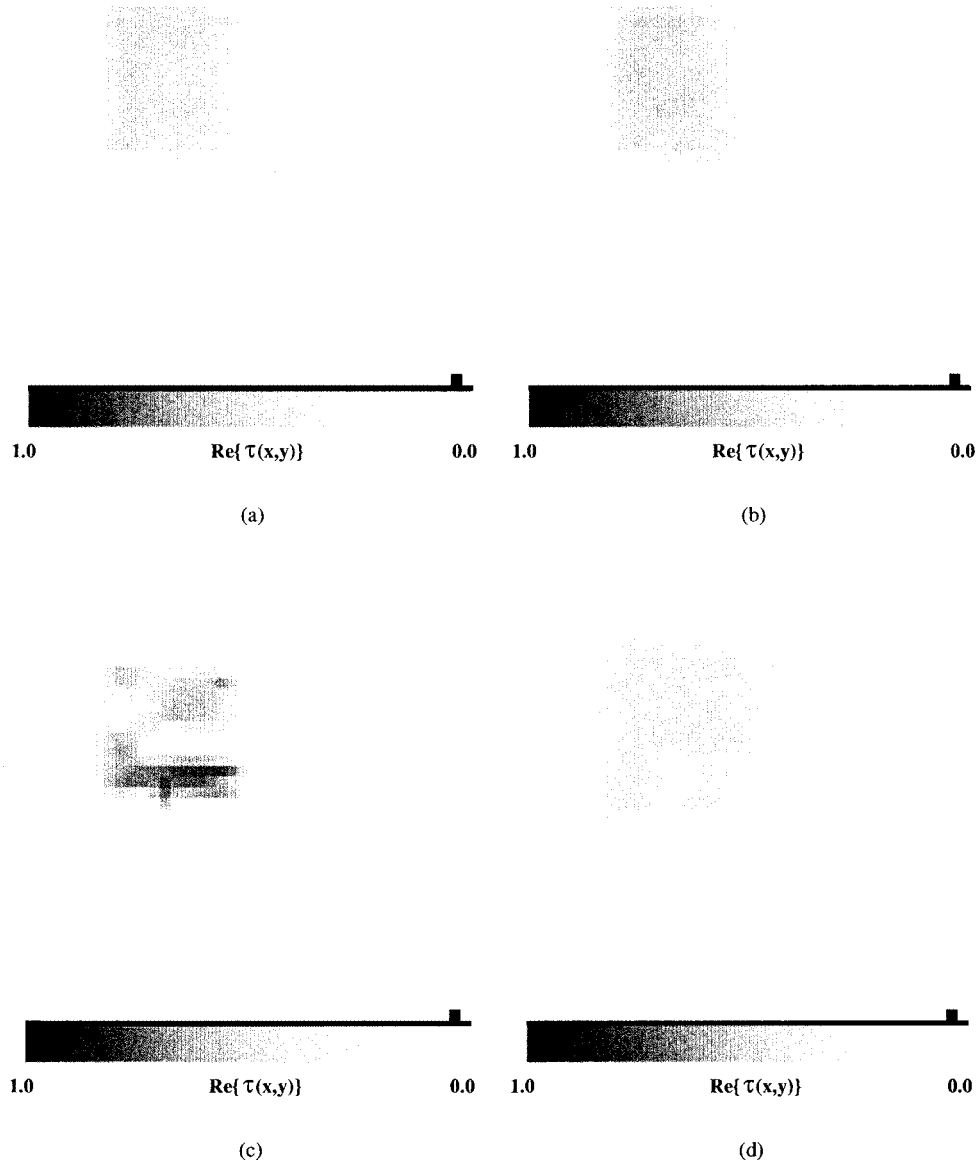

Fig. 5. Reconstruction of an off-centered square homogeneous cylinder. Retrieved profiles at $s = S_{\rm opt}$ when: (a) $\rm SNR = 30$ dB, (b) $\rm SNR = 20$ dB, (c) $\rm SNR = 10$ dB, (d) $\rm SNR = 5$ dB.

As far as the assessment of the effectiveness in the qualitative imaging of the geometry under test is concerned, the following parameters are defined:

$$\rho = \frac{\sqrt{\left[x_c^{(S_{\rm opt})} - x_c^{\rm ref}\right]^2 + \left[y_c^{(S_{\rm opt})} - y_c^{\rm ref}\right]^2}}{\lambda_0} \tag{11}$$

$$\Delta = \left\{\frac{L_{(S_{\rm opt})} - L_{\rm ref}}{L_{\rm ref}}\right\} \times 100. \tag{12}$$

The presence of a noisy environments is also taken into account by considering an additive Gaussian noise characterized by a signal-to-noise ratio (SNR) defined as follows:

$$\rm SNR = 10 \log \left\{ \frac{\sum_{v=1}^{V}\sum_{m=1}^{M}\left|E^v_{\rm scatt}\left(x_{m_{(v)}}, y_{m_{(v)}}\right)\right|^2}{\sum_{v=1}^{V}\sum_{m=1}^{M}\left|\mu\left(x_{m_{(v)}}, y_{m_{(v)}}\right)\right|^2} \right\} \tag{13}$$

with μ being a complex Gaussian random variable with zero mean value.

B. Homogeneous Square Cylinder

In the first example, a lossless square scatterer $L = 0.8\ \lambda_0$-sided, belonging to an inaccessible square investigation domain ($L_D = 2.4\ \lambda_0$), is located at $x_c^{\rm ref} = -y_c^{\rm ref} = 0.4\ \lambda_0$. The object is characterized by an homogeneous distribution of the object function $\tau = 0.5 + j0.0$ [see Fig. 3(a)]. A set of $V = 4$ unit TM plane waves (whose incident angles are given by $\theta^v_{\rm inc} = (v-1)\pi/2,\ v = 1, \ldots, V$) illuminated the investigation domain. For each illumination, the scattered electric field data have been collected at $M = 21$ equally spaced detectors located on a circle $\rho^v_m = 1.8\ \lambda_0$ in radius belonging to the observation domain. As far as the inversion data are concerned, the values of the scattered field $E^v_{\rm scatt}\left(x_{m_{(v)}}, y_{m_{(v)}}\right)$ have been synthetically computed by using Richmond's procedure

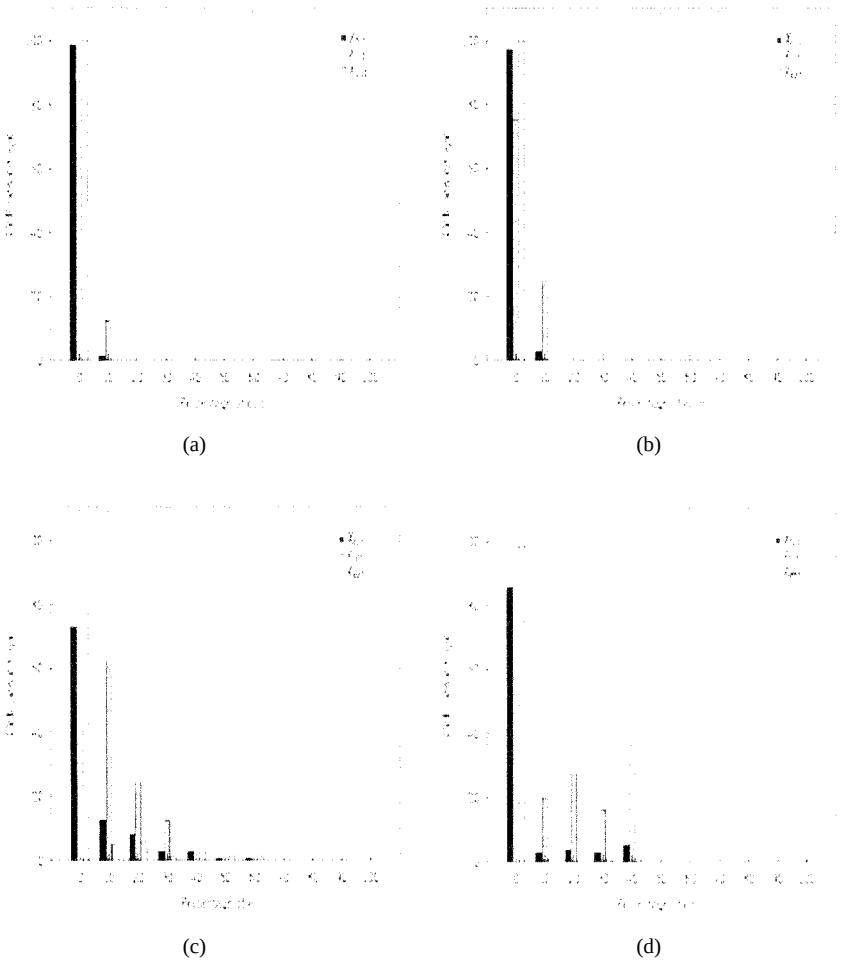

(a) (b) (c) (d)

Fig. 6. Reconstruction of an off-centered square homogeneous cylinder (noisy data). Local error behavior when: (a) $\mathrm{SNR} = 100$ dB, (b) $\mathrm{SNR} = 20$ dB, (c) $\mathrm{SNR} = 10$ dB, (d) $\mathrm{SNR} = 5$ dB.

[27]. However, in order to avoid the so-called "inverse crime problem" [28], a different discretization of the investigation domain have been used for the direct procedure.

Fig. 3 shows the evolution of the reconstruction obtained by means of the iterative multiscaling approach. At the first step ($s = 1$), the investigation domain is partitioned into $N_1 = 36$ square subdomains ($l_2 = 0.4\ \lambda_0$) and the guess dielectric distribution is equal to the background ($\tau = \tau_0$).

At the end of the minimization process relative to the first step (performed by means of a conjugate-gradient-based procedure and stopped when a "stationary condition" in the decrease of the cost function is achieved (see Fig. 4), the scatterer is roughly localized ($x_c^{(1)} = -y_c^{(1)} = -0.22\ \lambda_0$) and shaped [see Fig. 3(b)]. A reduced investigation domain $L_{(1)} = 1.76\ \lambda_0$ in side (Table I) is then defined.

At the second step, two different subgridding are used, the finer resolution is used for the reduced investigation domain found at the previous step. The reduced area is again discretized into $N_2 = 36$ square subdomains $l_2 = 0.29\ \lambda_0$ in side. Fig. 3(c) shows the object profile retrieved at the end of the minimization process of the second step. The multiscaling iterative procedure is repeated until $s = S_{\mathrm{opt}} = 3$ when fixed thresholds (empirically stated and equal to $\eta_x = 1\%$, $\eta_y = 1\%$, and $\eta_L = 5\%$) are reached. The unknown target results correctly located ($x_c^{(3)} = -0.397\ \lambda_0$, $y_c^{(3)} = 0.397\ \lambda_0$) and the occupation area of the actual object are estimated with a good accuracy ($L_3 = 0.86\ \lambda_0$). The method also provides a good reconstruction, as confirmed from the values of the error figures (Table II) which, at the final step, result in no greater than 1.5%.

For the same configuration, the effects of the noise have been taken into account. To this end, a Gaussian noise has been added to the data. The noise level ranges from 30 up to 5 dB. Fig. 5 gives a representation of the reconstructed contrast for different SNR. The final convergent solutions for SNR from 30 to 10 dB are reached after three scaling steps. Two steps are necessary when $\mathrm{SNR} = 5$ dB. As can be observed, the multiscaling method appears to be reasonably stable with respect to the noise. It results in that only extremely high noise levels yield some anomalies [see Fig. 5(c)–(d)], but the location and shape of the scatterer are still visible in the reconstructed profile.

As far as the quantitative and qualitative imaging of the scatterer is concerned, some information about the error distribution can be inferred from Fig. 6 where the histograms of the behavior of the local error are reported.

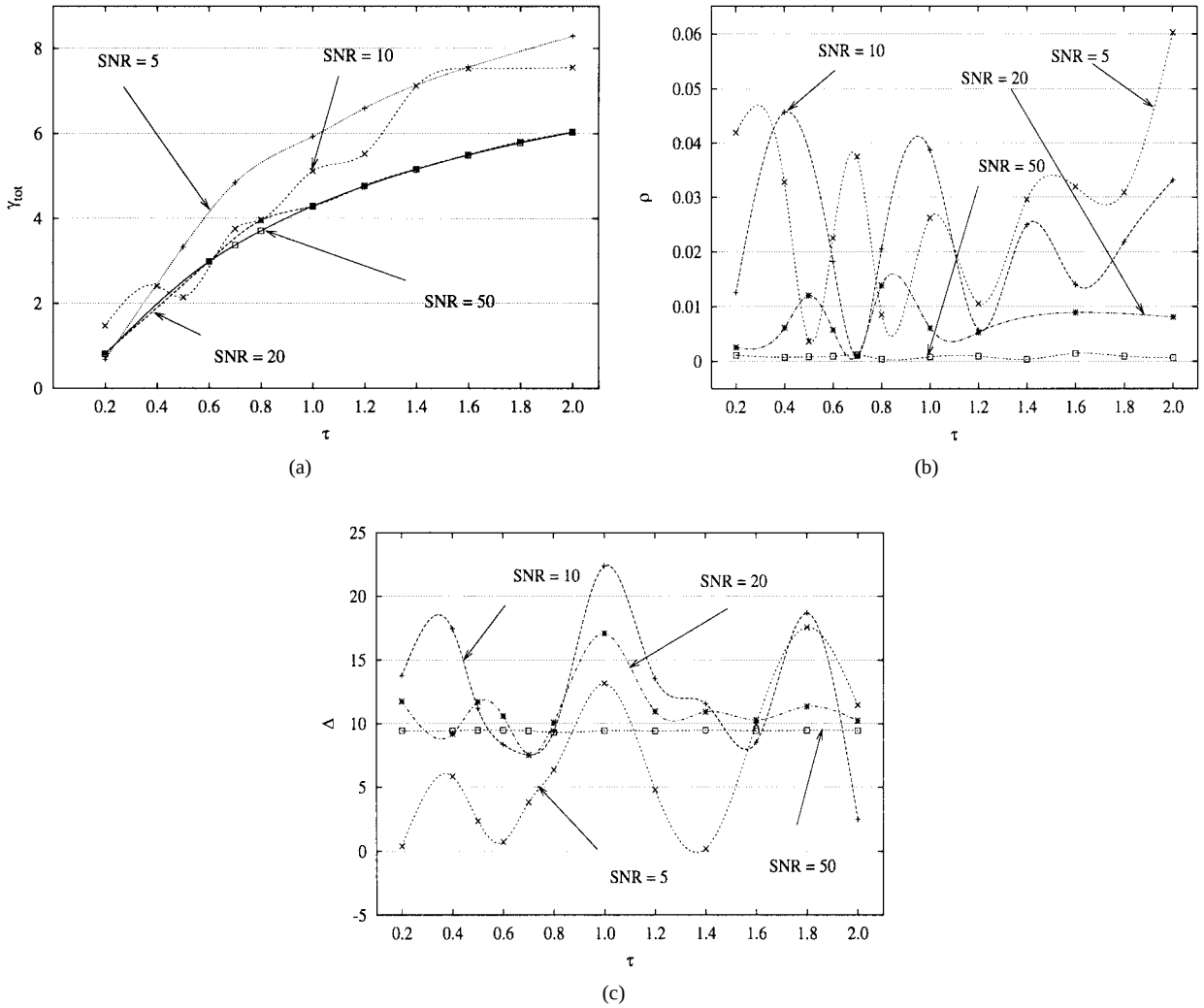

Fig. 7. Reconstruction of an off-centered square homogeneous cylinder. Dependence of the: (a) reconstruction accuracy, (b) scatterer location, and (c) object shaping from the scatterer's dimensions.

Each bar of the histogram gives the percentage of cells for which the local error χ (being $\chi_{\rm tot}$, $\chi_{\rm int}$, and $\chi_{\rm ext}$ related to the whole scattering domain, inside and outside the object support, respectively) is negligible, between 3%–10%, 10%–20%, and so on. For low noise levels ($\mathrm{SNR} > 20$ dB), approximately 100% of the cells are without error ($\chi_{\rm tot} \leq 3\%$) and the internal local error results are lower than 10% . When the SNR decreases, the local error increases. The quantitative imaging does not result as accurately, as confirmed from the gray-level representation given in Fig. 5(c) and (d). Almost every cell belonging to the area of the actual scatterer is affected by an error. However, the local error is less than 3% in a large amount of the cells outside the scatterer. This further confirms the effectiveness of the multiresolution procedure in locating and shaping the target under test. In order to evaluate the effect of the scatterer's dielectric permittivity on the reconstruction process, some simulations have also been performed. To this end, the dimensions and characteristics of the observation domain have been assumed as those used in the first simulation, while the value of the relative dielectric permittivity of the object has been varied between $\varepsilon_r = 1.2$ and $\varepsilon_r = 3.0$. The quantitative and qualitative imaging capabilities of the proposed procedure can be inferred by observing Fig. 7 where the plots of $\gamma_{\rm tot}$, ρ, and Δ are given. As far as the reconstruction of the dielectric profile is concerned, a good accuracy ($\gamma_{\rm tot} \leq 8$) is achieved in the whole range of variations of ε_r and for each SNR [see Fig. 8(a)]. Starting from $\mathrm{Re}(\tau) \cong 1.2$, the location error strongly depends on the value of SNR, but, in any case, ρ results are lower than 6% [see Fig. 8(b)]. On the other hand, the error in estimating the occupation area of the scatterer is limited to the range between 5%–20%. It assumes a constant value ($\Delta \cong 9\%$) when the measurement environment is characterized by a low noise level ($\mathrm{SNR} = 50$ dB) [see Fig. 8(c)].

To further assess the capabilities of a microwave imaging procedure, it should be taken into account that the size of the object under test could affect the validity of the inversion procedure. Consequently, another set of simulations has been carried out in order to evaluate the suitability of the multiscaling methodology to deal with smaller as well larger (compared to the background wavelength) scatterers. The area of the square scatterer ($\varepsilon_r = 1.5$) has been varied continuously in the range between $A = 0.1\,\lambda_0^2$ to $A = 2.8\,\lambda_0^2$ and various measurement conditions have been taken into account ($\mathrm{SNR} = 0.5 \div 100$ dB).

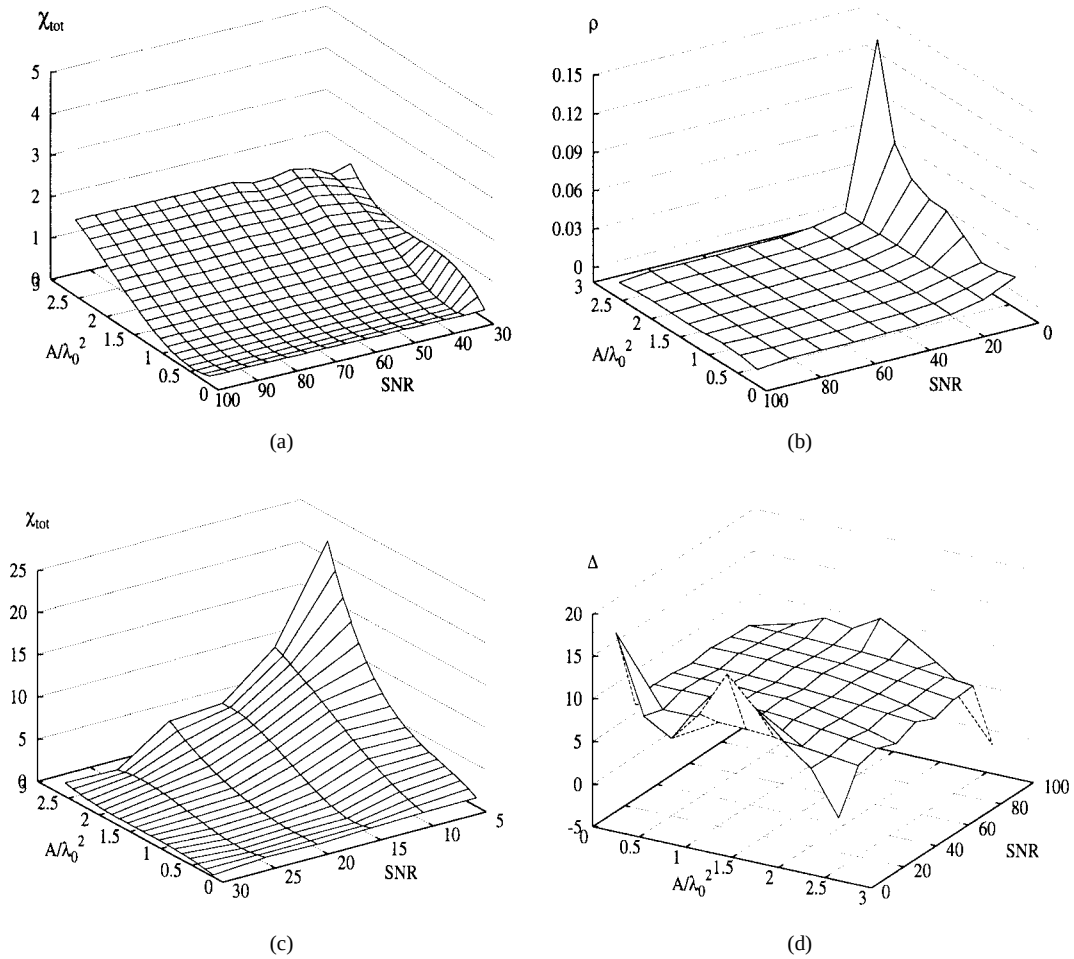

Fig. 8. Reconstruction of an off-centered square homogeneous cylinder ($\varepsilon_r = 1.5$). Dependence of the: (a) reconstruction accuracy, (b) scatterer location, and (c) object shaping from the scatterer's dimensions.

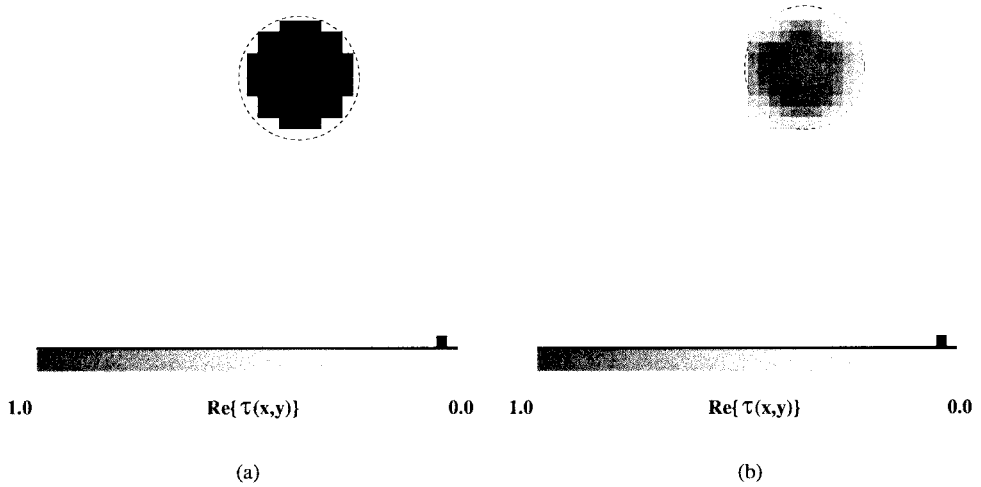

Fig. 9. Reconstruction of a circular homogeneous cylinder (Noiseless conditions). (a) Reference profile and (b) retrieved profile ($s = S_{\rm opt} = 3$).

Fig. 8 shows a pictorial representation of the error figures for different values of the scatterer area and for various SNRs. Starting from Fig. 8(a), we can observe that when $\mathrm{SNR} > 25\,\mathrm{dB}$, the reconstruction error is lower than 2% whatever the object dimensions. On the contrary, when the signal to noise increases, $\gamma_{\rm tot}$ strongly depends to the scatterer area. As an example, assuming $\mathrm{SNR} = 10$ dB, the reconstruction error ranges from 2% to 10%. As far as the behavior of ρ is concerned, Fig. 8(b) clearly indicates that the method is able to accurately locate the position of the scatterer ($\rho \leq 0.010$ when $\mathrm{SNR} \geq 10$ dB).

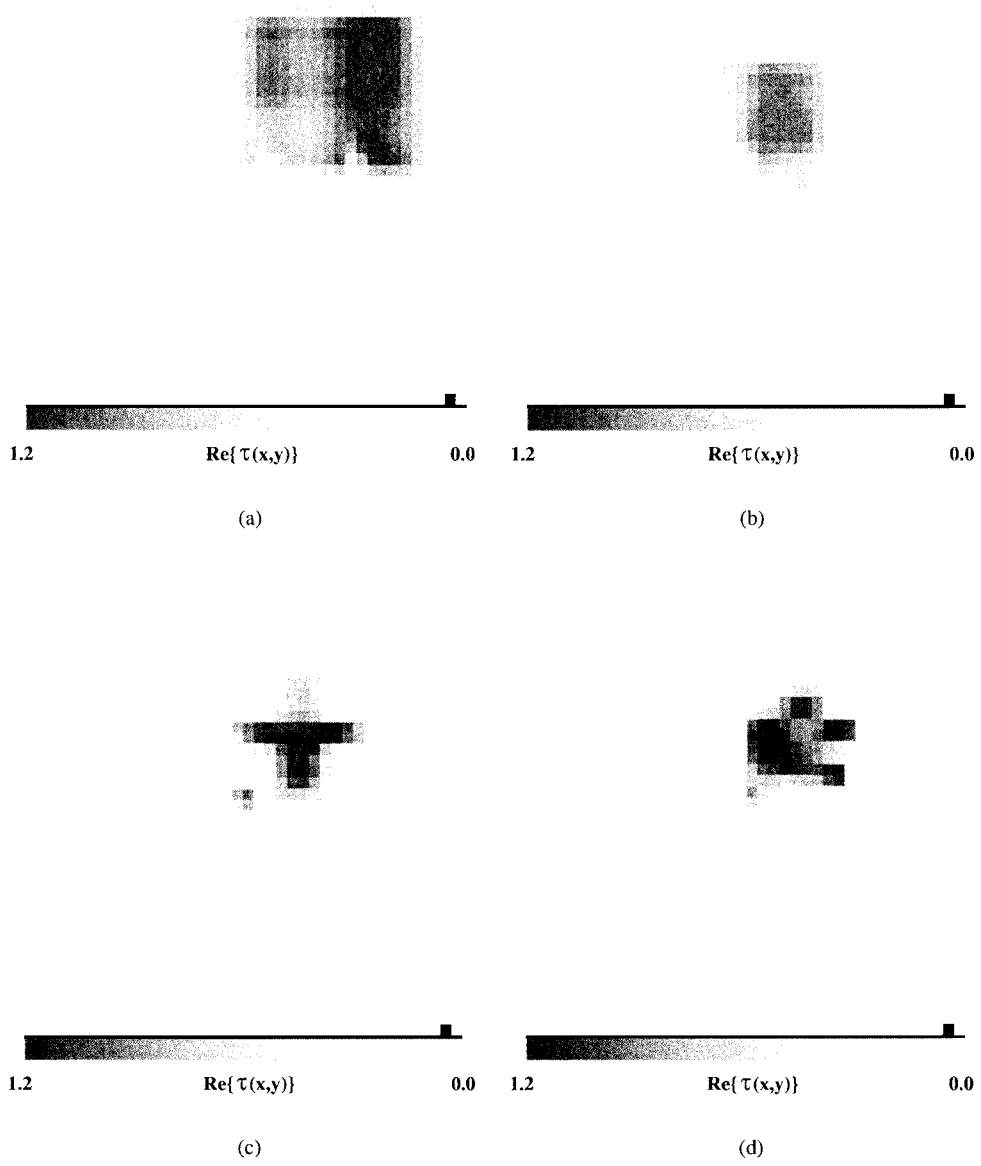

Fig. 10. Reconstruction of a circular homogeneous cylinder (Noisy conditions). Reconstruction at intermediate steps: (a) $s = 1$, (b) $s = 2$, and (c) $s = 3$. (c) Final convergent profile ($s = S_{\rm opt} = 4$).

TABLE III
RECONSTRUCTION OF A CIRCULAR HOMOGENEOUS CYLINDER. BEHAVIOR OF THE STATIONARY INDEXES AND ERROR FIGURES FOR MULTISCALING AND STANDARD NONLINEAR INVERSE-SCATTERING PROCEDURE, RESPECTIVELY

	Multi-scaling Procedure				Single-step Procedure
Step No. (s)	*1*	*2*	*3*	*4*	*1*
$\eta_x^{(s)}$	8.07	4.48	0.098	0.062	28.6
$\eta_y^{(s)}$	14.81	0.38	5.84	0.989	21.3
$\eta_L^{(s)}$	40.56	21.35	11.33	3.18	46.4
γ_{tot}	10.692	4.258	3.477	2.218	3.26
γ_{int}	15.295	7.076	13.491	9.202	15.86
γ_{ext}	10.535	4.162	3.134	1.979	2.59

Generally, the dimensions of the target are also correctly estimated. The occupation area error results equal to $\sim 7.5\%$ independently of scatterer's dimensions and noisy conditions.

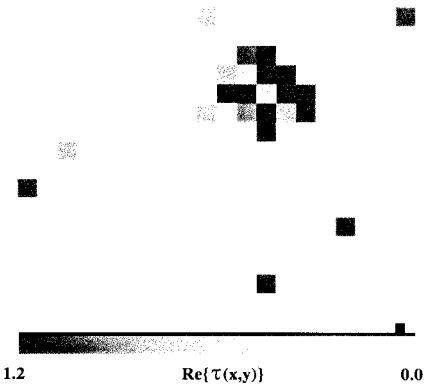

Fig. 11. Reconstruction of a circular homogeneous cylinder by means of a standard nonlinear inverse-scattering method (noisy condition).

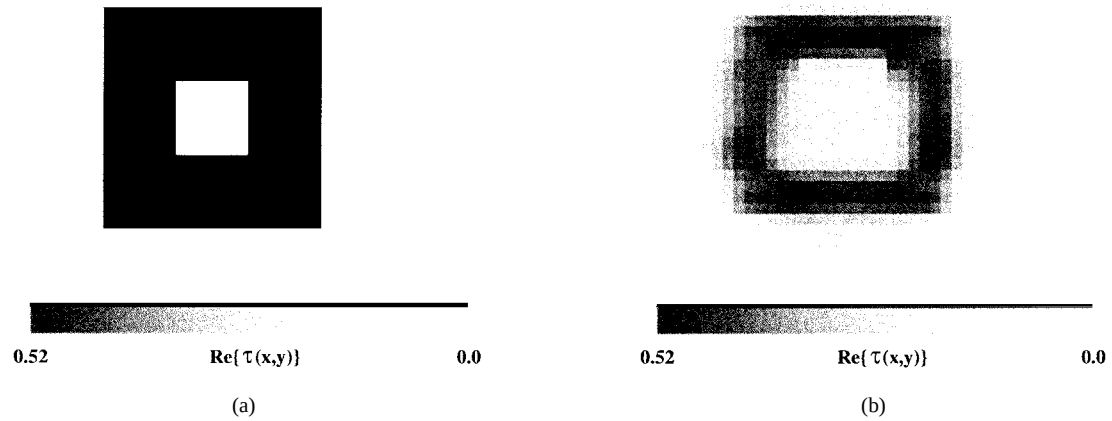

Fig. 12. Reconstruction of a two-layer square cylinder ($L_{\rm out} = 1.2\ \lambda_0$ and $L_{\rm in} = 0.4\ \lambda_0$). (a) Reference profile and (b) retrieved profile ($s = S_{\rm opt} = 3$).

C. Circular Cylinder

In this section, a dielectric profile, for which an analytical solution for the computation of scattered field is available, is considered. An off-centered ($x_c^{\rm ref} = y_c^{\rm ref} = 0.3\ \lambda_0$) circular dielectric cylinder with a relative dielectric permittivity $\varepsilon_r(x,y) = 2.0, 0.3\ \lambda$ in radius has been located in the investigation domain. In the first set of numerical simulations, a noiseless environment has been assumed. During the reconstruction process, $\mathrm{Re}\{\tau(x,y)\}$ can range between 0.0–2.0. Fig. 9 shows a grey-level representation of the dielectric distribution of the scatterer under test retrieved at the final step ($S_{\rm opt} = 3$) of the multiresolution procedure. The actual distribution is also shown [see Fig. 9(a)]. As can be observed, the object is correctly located ($x_{c_{(S_{\rm opt})}} = 0.301\ \lambda_0$ and $y_{c_{(S_{\rm opt})}} = 0.298\ \lambda_0$), shaped ($L_{(S_{\rm opt})}/2 = 0.324\ \lambda_0$), and reconstructed ($\gamma_{\rm int} = 9.022$).

Successively, a Gaussian noise characterized by an $\mathrm{SNR} = 10$ dB has been added to the simulated scattered field at the measurement points. Fig. 10 shows the reconstructed results at the end of each step of the multiresolution procedure. The final ($S_{\rm opt} = 4$ being $\eta_x^{(4)} < \eta_x$, $\eta_y^{(4)} < \eta_y$, and $\eta_L^{(4)} < \eta_L$) retrieved dielectric profile is reported in Fig. 10(d).

As expected, the presence of the noise causes a deterioration of the reconstruction accuracy (the maximum value of the dielectric permittivity is estimated to be equal to $\max_{(x,y)\in D}\{\varepsilon_r(x,y)\} = 2.1$), however, the values of the error figures (Table III) result is acceptable also taking into account the high noise level.

For comparison purposes and in order to point out the real advantages of the multistep approach over standard nonlinear inverse-scattering methods, the same reconstruction has been performed by using a single-step minimization with the conjugate gradient method. To this end, as far as the single-step procedure is concerned, the investigation domain has been discretized with an homogeneous grid whose cell side is equal to the finer discretization step of the multiscaling procedure ($l_4 = 0.12\ \lambda_0$). As can be observed (Fig. 11), the reconstructed profile presents some artifacts and neither the center, nor the shape of the scatterer under test are correctly estimated, as confirmed in Table III, where the error figures are reported and compared with those achieved with the multistep procedure. Moreover, the new methodology allows a significant computational saving. The computational effort for the new method is substantially lower so that more accurate reconstruction results can be achieved in approximately 1/4 of the time required for the standard algorithm. In more detail, each iteration of the standard algorithm took approximately 6 s on a Pentium III 1.2 GHz (Linux OS) when an iteration of the multiscaling requires only 0.12 s.

TABLE IV
RECONSTRUCTION OF TWO-LAYER SQUARE CYLINDER. ERROR FIGURES

	Two-layered Square Cylinder	
	$L_{out} = 1.2\,\lambda_0$ - $L_{in} = 0.4\,\lambda_0$	$L_{out} = 1.6\,\lambda_0$ - $L_{in} = 0.8\,\lambda_0$
γ_{tot}	5.961	4.640
γ_{int}	12.150	5.017
γ_{ext}	4.316	1.39

D. Hollow Square Scatterer

Finally, the reconstruction of a slightly complex cylindrical object is taken into account. The target is an off-centered square two-layer cylinder ($x_c^{\rm ref} = y_c^{\rm ref} - 0.2\lambda_0$). The inner square, characterized by a permittivity equal to that of the background, is $0.4\,\lambda_0$-sided. The side of the outer cylinder ($\tau(x,y) = 0.5$) is equal to $1.2\ \lambda_0$. As far as the noisy environment is concerned, an SNR $\mathrm{SNR} = 30$ dB has been assumed.

Fig. 12 shows the reference and reconstructed object function distribution inside the investigation domain, respectively. As can be noted, the scatterer is accurately localized and quite correctly shaped. However, the side of the square scatterer is slightly overestimated as well as the value of $\mathrm{Re}(\tau)$ of the inner cylinder. These conclusions are confirmed from the values of the error figures reported in Table IV.

On the other hand, when the dimensions of the inner cylinder ($L_{\rm out} = 1.6\ \lambda_0$ and $L_{\rm in} = 0.8\ \lambda_0$) increases, the quality of the reconstruction of the scatterer under test also improves (Fig. 13), as confirmed from the error figures (Table IV).

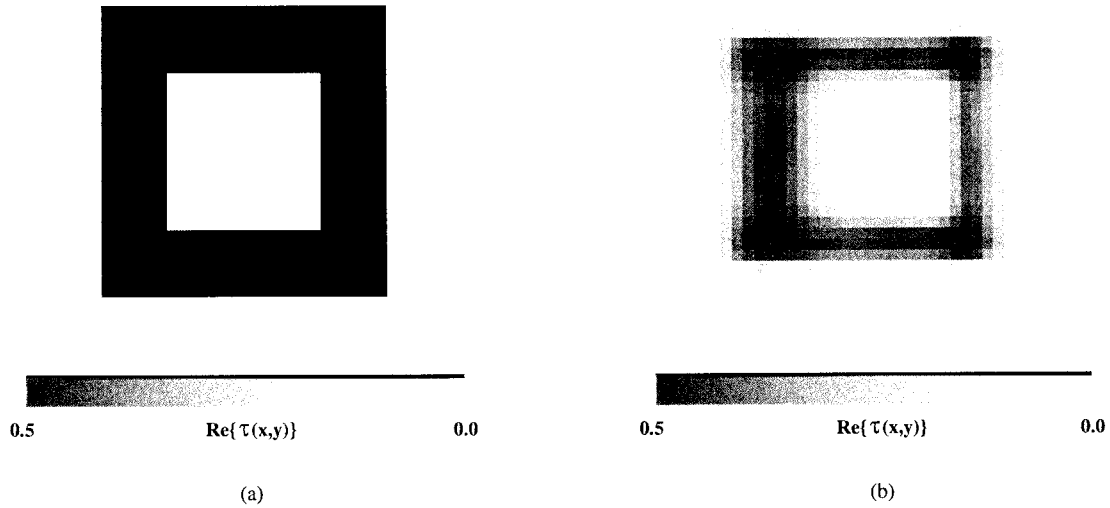

Fig. 13. Reconstruction of a two-layer square cylinder ($L_{\rm out} = 1.6\ \lambda_0$ and $L_{\rm in} = 0.8\ \lambda_0$). (a) Reference profile and (b) retrieved profile ($s = S_{\rm opt} = 4$).

IV. Conclusion

An innovative methodology for reconstructing the dielectric permittivity distribution of cylindrical scatterers has been presented. The procedure, based on a multilevel resolution algorithm, is aimed at better exploiting the limited amount of the information achievable from the scattering measurement. To this end, a suitable iteratively defined (according to the information about the scatterer collected at the previous steps) cost function is successively minimized by means of an optimization method. A conjugate-gradient-based method has been used, but, in principle, any kind of optimization technique could be successfully adopted. The proposed approach, developed in the spatial domain and under TM illumination conditions, has been assessed by means of some test cases and the obtained results have shown its capabilities in imaging simple objects, even in strongly noisy environments. In more detail, numerical simulations have been carried out to test the behavior of the multiresolution procedure when some parameters (e.g., scatterer dimensions, dielectric permittivity, scatterer shapes, etc.) of the scenario under test are changed. Results are quite promising and indicate that the new methodology exhibits the best features of the minimized algorithm (which, actually, constitutes a "*black box*" inside the overall system), but also additional properties in term of convergence rate, memory requirements, and reconstruction accuracy.

However, the proposed scheme must be further improved by overcoming some current limitations. In particular, two key points should be addressed: the occurrence of local minima and the improvement of the stopping criterion (or "stationary condition"). As far as the "*local minima*" problem is concerned, certainly the multiscaling method considerably reduces (with respect to deterministic inverse-scattering methods) the risk that the trial solution be trapped in a local minimum. However, there is no guarantee of avoiding local minima if the minimization procedure is a deterministic algorithm. To this end, a modified version of the multistep procedure is currently under development, which considers a stochastic minimization procedure. As far as the stopping criterion is concerned, heuristic thresholds are currently taken into account. No deep studies have been carried out about the dependence of these parameters on the characteristics of the scenario under test. To this end, an accurate analysis is currently performed in order to define an analytic rule for the threshold definition by including in an efficient way all the available *a priori* information.

References

[1] W. Tabbara, B. Beuchene, C. Pichot, D. Lesselier, L. Chommeloux, and N. Joachimowicz, "Diffraction tomography: Contribution to the analysis of applications in microwave and ultrasonics," *Inverse Problems*, vol. 4, pp. 305–331, 1988.

[2] D. Colton and R. Krees, *Inverse Acoustics and Electromagnetic Scattering Theory*. Berlin, Germany: Springer-Verlag, 1992.

[3] M. Bertero and E. R. Pike, *Inverse Problems in Scattering and Imaging*. U.K.: Adam Hilger, 1992.

[4] T. M. Habashy, M. L. Oristaglio, and A. T. de Hoop, "Simultaneous non linear reconstruction of two-dimensional permittivity and conductivity," *Radio Sci.*, vol. 29, pp. 1101–1118, 1994.

[5] J. C. Bolomey *et al.*, "Microwave diffraction tomography for biomedical applications," *IEEE Trans. Microwave Theory Tech.*, vol. MTT-30, pp. 1998–2000, Nov. 1982.

[6] A. K. Louis, "Medical imaging: State of the art and future development," *Inverse Problems*, vol. 8, pp. 709–738, 1992.

[7] R. L. Barbour, M. J. Carvlin, and M. A. Fiddy, "Experimental and numerical methods for solving ill-posed inverse problems: Medical and non medical applications," in *Proc. SPIE*, vol. 2570, San Diego, CA, 1995.

[8] S. R. H. Hooley *et al.*, "Inverse problem methodology and finite elements in the identifications of cracks, sources, materials, and their geometry in inaccessible locations," *IEEE Trans. Magn.*, vol. 27, pp. 3433–3443, May 1991.

[9] A. C. Dubey *et al.*, "Detection technology for mines and minelike targets," in *Proc. SPIE*, vol. 2496, Orlando, FL, 1995.

[10] K. M. Golden *et al.*, "Inverse electromagnetic scattering models for sea ice," *IEEE Trans. Geosci. Remote Sensing*, vol. 36, pp. 1675–1704, Sept. 1998.

[11] A. Quing and L. Jen, "Microwave imaging of dielectric cylinder in layered media," *J. Electromagn. Waves Applicat.*, vol. 11, no. 2, pp. 259–269, 1997.

[12] J. C. Bolomey, "Recent European developments in active microwave imaging for industrial, scientific and medical applications," *IEEE Trans. Microwave Theory Tech.*, vol. 37, pp. 2109–2117, June 1989.

[13] B. D. Steinberg, *Microwave Imaging Techniques*. New York: Wiley, 1991.

[14] A. Kirsch, *An Introduction to the Mathematical Theory of Inverse Problems*. New York: Springer-Verlag, 1996.

[15] A. M. Denisov, *Elements of Theory of Inverse Problems*. Utrecht, The Netherlands: VSP, 1999.

[16] D. Colton and L. Paivarinta, "The uniqueness of a solution to an inverse scattering problem for electromagnetic waves," *Arc. Ration. Mech. Anal.*, vol. 119, pp. 59–70, 1992.

[17] V. Isakov, "Uniqueness and stability in multidimensional inverse problems," *Inverse Problems*, vol. 9, pp. 579–621, 1993.
[18] M. Slaney, A. C. Kak, and L. E. Larsen, "Limitations of imaging with first-order diffraction tomography," *IEEE Microwave Theory Tech.*, vol. MTT-32, pp. 860–874, Aug. 1984.
[19] R. E. Kleinman and P. M. Ven den Berg, "A modified gradient method for two-dimensional problems in tomography," *J. Comput. Appl. Math.*, vol. 42, pp. 17–35, 1992.
[20] W. C. Chew and Y. M. Wang, "Reconstruction of two-dimensional permittivity distribution using the distorted Born iterative method," *IEEE Trans. Med. Imag.*, vol. 9, pp. 218–225, June 1990.
[21] L. Garnero, A. Franchois, J.-P. Hugonin, C. Pichot, and N. Joachimowicz, "Microwave imaging—Complex permittivity reconstruction by simulated annealing," *IEEE Trans. Microwave Theory Tech.*, vol. 39, pp. 1801–1807, Nov. 1991.
[22] A. Massa, "Genetic algorithm based techniques for 2D microwave inverse scattering," in *Recent Research Developments in Microwave Theory and Techniques*, S. G. Pandalai, Ed. Trivandrum, India: Transworld Res. Network Press, 2002.
[23] M. Pastorino, A. Massa, and S. Caorsi, "A microwave inverse scattering technique for image reconstruction based on a genetic algorithm," *IEEE Trans. Meas. Instrum.*, vol. 49, pp. 573–578, June 2000.
[24] M. Bertero, C. De Mol, and E. R. Pike, "Linear inverse problems with discrete data. I: General formulation and singular system analysis," *Inverse Problems*, vol. 1, pp. 301–330, 1995.
[25] M. Bertero and P. Boccacci, *Introduction to Inverse Problems in Imaging*. Bristol, U.K.: IOP, 1998.
[26] C. Pichot, P. Lobel, C. Dourthe, L. B. Féraud, and M. Barlaud, "Microwave inverse scattering: Quantitative reconstruction of complex permittivity for different applications," *IEICE Trans. Electron.*, vol. E80-C, pp. 1343–1348, 1997.
[27] J. H. Richmond, "Scattering by a dielectric cylinder of arbitrary cross section shape," *IEEE Trans. Antennas Propagat.*, vol. AP-13, pp. 334–341, May 1965.
[28] D. Colton and R. Kress, *Inverse Acoustic and Electromagnetic Scattering Theory*. Berlin, Germany: Springer-Verlag, 1992.
[29] K. Belkebir, R. E. Kleinman, and C. Pichot, "Microwave imaging location and shape reconstruction from multifrequency scattering data," *IEEE Trans. Microwave Theory Tech.*, vol. 45, pp. 469–476, Apr. 1997.
[30] H. Harada, D. J. N. Wall, T. T. Takenaka, and T. Tanaka, "Conjugate gradient method applied to inverse scattering problems," *IEEE Trans. Antennas Propagat.*, vol. 43, pp. 784–792, Aug. 1995.
[31] S. Caorsi, A. Massa, and M. Pastorino, "A computational technique based on a real-coded genetic algorithm for microwave imaging purposes," *IEEE Trans. Geosci. Remote Sensing (Special Issue)*, vol. 38, pp. 1697–1708, July 2000.

Salvatore Caorsi (M'98) received the Laurea degree in electronic engineering from the University of Genoa, Genoa, Italy, in 1973.

Upon graduation, he remained with the University of Genoa as a Researcher and, since 1976, he has been a Professor of antennas and propagation. In 1985, he also became a Professor of fundamentals of remote sensing. Since 1994, he has been a Full Professor of electromagnetic compatibility with the Department of Electronics, University of Pavia, Pavia, Italy. He is the past Chairman of the Inter-university Research Center for Interactions Between Electromagnetic Fields and Biological Systems (ICEMB). His primary activities are focused on applications of electromagnetic fields to telecommunications, artificial vision and remote sensing, biology, and medicine. In particular, he is currently involved with research projects concerning microwave hyperthermia and radiometry in oncological therapy, numerical methods for solving electromagnetic problems, and inverse scattering and microwave imaging.

Dr. Caorsi is a member of the Associazione Elettrotecnica ed Elettronica Italiana (AEI), the European Bioelectromagnetism Association (EBEA), and the European Society for Hyperthermic Oncology (ESHO).

Massimo Donelli was born in Genoa, Italy, in 1972. He received the Electronic Engineering degree from the University of Genoa, Genoa, Italy, in 1998, and is currently working toward the Ph.D. degree in science and engineering for space with the University of Genoa.

He is currently with the Department of Biophysical and Electronic Engineering, University of Genoa. His area of interest concerns electromagnetic compatibility, electromagnetic modeling, and numerical methods in electromagnetic.

Davide Franceschini was born in Trento, Italy, in 1979. He received the Laurea degree in telecommunication engineering from the University of Trento, Trento, Italy, in 2002.

His main interests are electromagnetic inverse scattering and optimization techniques for microwave imaging.

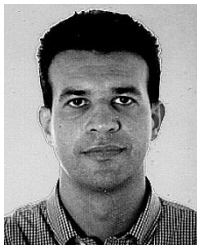

Andrea Massa (M'01) received the Laurea degree in electronic engineering and Ph.D. degree in electronics and computer science from the University of Genoa, Genoa, Italy, in 1992 and 1996, respectively.

From 1997 to 1999, he was an Assistant Professor of electromagnetic fields with the Department of Biophysical and Electronic Engineering, University of Genoa, where he taught "Electromagnetic Fields 1." He is currently an Associate Professor with the University of Trento, Trento, Italy, where he teaches "Electromagnetic Fields" and "Electromagnetic Diagnostic Techniques." He is a member of the Inter-university Research Center for Interactions Between Electromagnetic Fields and Biological Systems (ICEmB). Since 1992, his research has principally concerned electromagnetic direct and inverse scattering, optimization techniques for microwave imaging, wave propagation in the presence of nonlinear media, applications of electromagnetic fields to telecommunications, medicine, and biology.